JOURNAL OF GEOPHYSICAL RESEARCH, VOL. 100, NO. B4, PAGES 6295–6312, APRIL 10, 1995

Three-dimensional modeling of pull-apart basins: Implications for the tectonics of the Dead Sea Basin

Rafael Katzman[1]

Department of Earth, Atmospheric and Planetary Sciences, Massachusetts Institute of Technology, Cambridge

Uri S. ten Brink

U.S. Geological Survey, Woods Hole, Massachusetts

Jian Lin

Department of Geology and Geophysics, Woods Hole Oceanographic Institution, Woods Hole, Massachusetts

Abstract. We model the three-dimensional (3-D) crustal deformation in a deep pull-apart basin as a result of relative plate motion along a transform system and compare the results to the tectonics of the Dead Sea Basin. The brittle upper crust is modeled by a boundary element technique as an elastic block, broken by two en echelon semi-infinite vertical faults. The deformation is caused by a horizontal displacement that is imposed everywhere at the bottom of the block except in a stress-free "shear zone" in the vicinity of the fault zone. The bottom displacement represents the regional relative plate motion. Results show that the basin deformation depends critically on the width of the shear zone and on the amount of overlap between basin-bounding faults. As the width of the shear zone increases, the depth of the basin decreases, the rotation around a vertical axis near the fault tips decreases, and the basin shape (the distribution of subsidence normalized by the maximum subsidence) becomes broader. In contrast, two-dimensional plane stress modeling predicts a basin shape that is independent of the width of the shear zone. Our models also predict full-graben profiles within the overlapped region between bounding faults and half-graben shapes elsewhere. Increasing overlap also decreases uplift near the fault tips and rotation of blocks within the basin. We suggest that the observed structure of the Dead Sea Basin can be described by a 3-D model having a large overlap (more than 30 km) that probably increased as the basin evolved as a result of a stable shear motion that was distributed laterally over 20 to 40 km.

Introduction

Pull-apart basins are structures associated with either right-lateral right-stepping or left-lateral left-stepping en echelon strike-slip faults, and are inherently three-dimensional (3-D) features. This work addresses the effect of regional tectonics and primary faulting on the deformation pattern of deep pull-apart basins using 3-D elastic modeling. 3-D numerical methods have been applied to crustal deformation problems only very recently [e.g., *Braun*, 1994; *Gomberg and Ellis*, 1994] . This study is the first attempt to model numerically pull-apart basins in three dimensions.

Several previous studies have examined the problem of pull-apart basins by using a two dimensional (2-D) plane stress solution. *Segall and Pollard* [1980] calculated the stress field due to the interaction between cracks that behave according to a linear frictional law in a 2-D elastic medium. *Bilham and King* [1989] and *Gomberg* [1993] used the 2-D boundary element technique to calculate the vertical strain around offsetting fault zones. A different approach by *Rodgers* [1980] used a superposition of analytical solutions for dislocation planes embedded in an elastic isotropic half-space [*Chinnery*, 1961, 1963]. *Rodgers* [1980] calculated the distribution of vertical displacement and stresses on the surface that results from two en echelon dislocations with no interaction between them.

In this study we use the boundary element method that has the advantage of addressing the boundary value problem by solving a system of coupled equations for elements that are distributed only on the boundary of the modeled region [*Crouch and Starfield*, 1983]. Since three-dimensional problems are reduced to two-dimensional in the boundary element method, this approach is more feasible than other methods for modeling problems with complex geometry. We use a 3-D commercial boundary element code, BEASY, that was developed by Computational Mechanics Inc., Billerica, Massachusetts. The accuracy of the algorithm is demonstrated in Appendix A by comparing analytical and numerical results for a simple half-space problem.

The need for a 3-D study is demonstrated by the significant differences predicted between a 3-D elastic plate model and a 2-D model with plane stresses for a pair of en echelon strike-slip faults (Figure 1). Results from the 3-D model show a single region of subsidence between the fault tips (Figure 1a). The 2-D results, on the other hand, show two asymmetric centers of

[1]Also at MIT/WHOI Joint Program in Oceanography, Massachusetts Institute of Technology, Cambridge.

Copyright 1995 by the American Geophysical Union.

Paper number 94JB03101.
0148-0227/95/94JB-03101$05.00

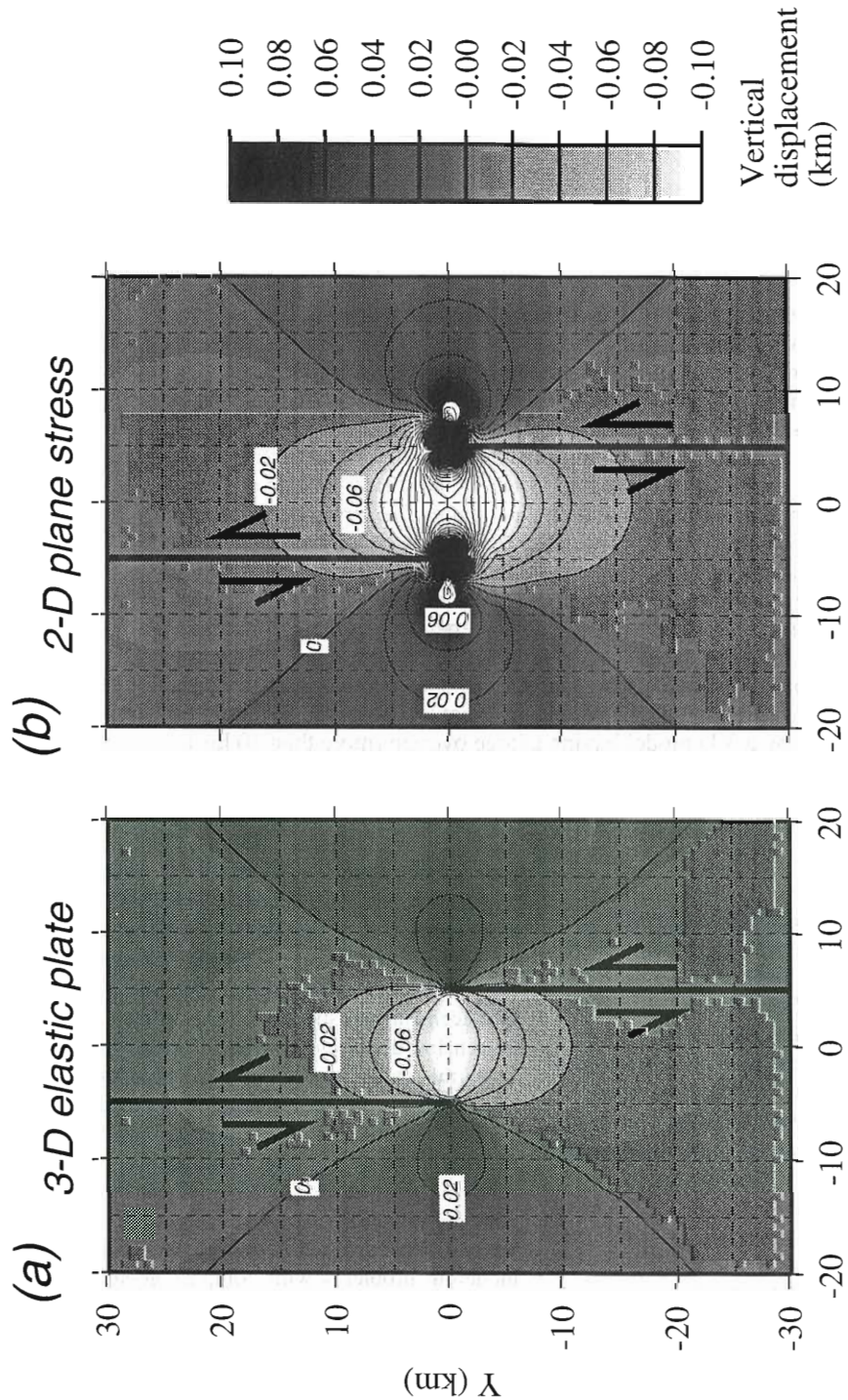

Figure 1. Comparison between 3-D and 2-D plane-stress models for pull-apart basins. Left-lateral displacement discontinuity of 1 km is explicitly defined across two en echelon, semi-infinite strike-slip faults (heavy lines) by two sets of elements that characterize the faults. Vertical displacement is shown for (a) a 3-D elastic plate with thickness of 15 km and (b) a 2-D thin elastic plate with elastic thickness of 15 km. Contour interval is 0.02 km. Poisson's ratio and Young's modulus in both models are 0.25 and 75 GPa, respectively.

subsidence near the fault tips that are too large to be geologicaly reasonable (15 times larger than maximum subsidence in the 3-D model) (Figure 1b). Previous workers [e.g., *Gomberg*, 1993] have tried to minimize the subsidence near the fault tips by introducing secondary faults to release the high strains or by tapering the slip near the tips of the primary faults. (Indeed, tapering the strains will help to reduce the large subsidence near the fault tips but will require an a priori knowledge of the tapering function and its relationship to a particular tectonic setting.) The large differences in vertical displacement between the 2-D and the 3-D solutions arise because the 2-D solution is based on a plane stress approximation that allows no vertical stresses to develop within the plate. Large vertical stresses do, however, develop in the center of the 3-D plate near the fault tips (Plate 1), which help support the plate against deformation there. Thus a 2-D plane stress solution is inaccurate close to the fault tips and produces an incorrect deformation pattern between the two en echelon faults.

The present view of the strength profile of the continental lithosphere [e.g., *Brace and Kohlstedt*, 1980] consists of a brittle upper crust with strength that linearly increases with depth [*Byerlee*, 1978] and an underlying much weaker ductile lower crust. The strongest part of the continental lithosphere, assuming a typical geotherm, lies in the uppermost mantle where the mantle temperature is the lowest and the mantle olivine strength is the greatest. A main premise of this study is that blocks separated by weak faults in the upper crust are driven from below by deformation of the continuum beneath them as the lithospheric plates are moving past each other [*Molnar*, 1992]. This lithospheric model serves as the basis for the boundary conditions that are applied in this work.

The upper crust is represented here by a three-dimensional elastic plate that is broken by vertical planes of weakness representing faults that cannot support any shear stresses (Figure 2). The regional motion of the lithospheric plates is represented by displacement applied at the bottom of the elastic plate. The basal displacement is applied everywhere except in a region of a finite width near the faults. We study the deformation pattern that develops in this zone of finite width (henceforth, "the shear zone", see Figure 2) as a result of regional relative plate motion and compare it to the tectonics of the Dead Sea Basin.

Our approach for modeling geological faults is somewhat different from the widely used approach in which a displacement discontinuity (dislocation) is explicitly defined on the fault plane [e.g., *Rodgers*, 1980; *Bilham and King*, 1989; *Gomberg*, 1993]. The dislocation approach used in these previous studies is useful because fault slip obtained from geological data can sometimes be directly embedded in the model. However, it is difficult to relate relative plate motion to slip on plate boundary faults and to determine a priori the tapering of the slip function toward the fault tips. In this study we use the dislocation approach mainly to address the difference between our results and the results of previous studies, but, because we do not know the appropriate slip function on the faults we use a constant slip in the same way as *Rodgers* [1980].

Perhaps the least palatable aspect of this work is the fact that linear elastic rheology is used for modeling finite deformation in the upper crust. In reality, but not in the models presented here, the rheology of the upper crust is elastic-plastic, which means that stresses increase with strains up to a certain limit, where failure occurs and plastic deformation starts. Beyond this limit, strains can increase significantly without a major change in the stresses. Our analysis is thus a linear approximation to a highly non linear process.

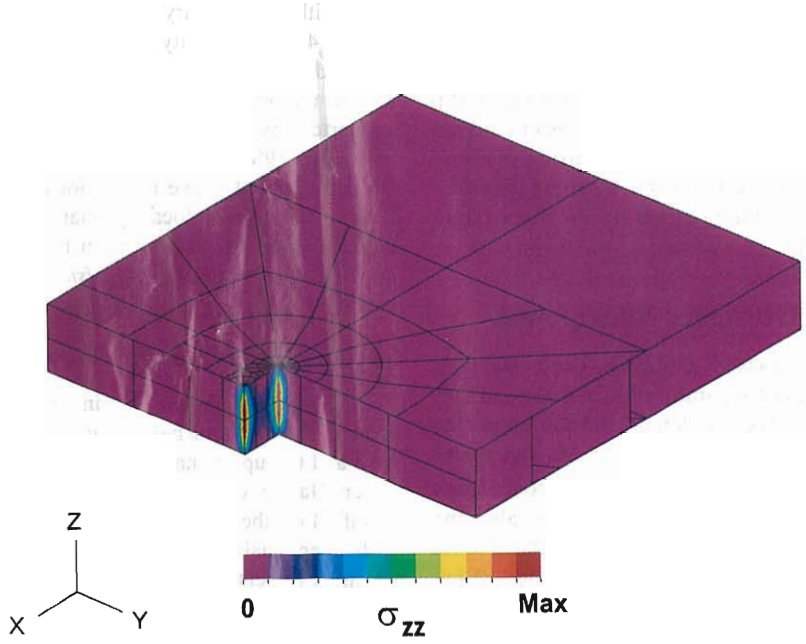

Plate 1. Three-dimensional block perspective of part of the elastic plate, cut along the en echelon faults, showing the vertical stresses σ_{zz} for the 3-D elastic plate model in Figure 1a. Note that significant vertical stresses develop near the fault tips unlike the plane stress assumption made in the 2-D modeling (Figure 1b).

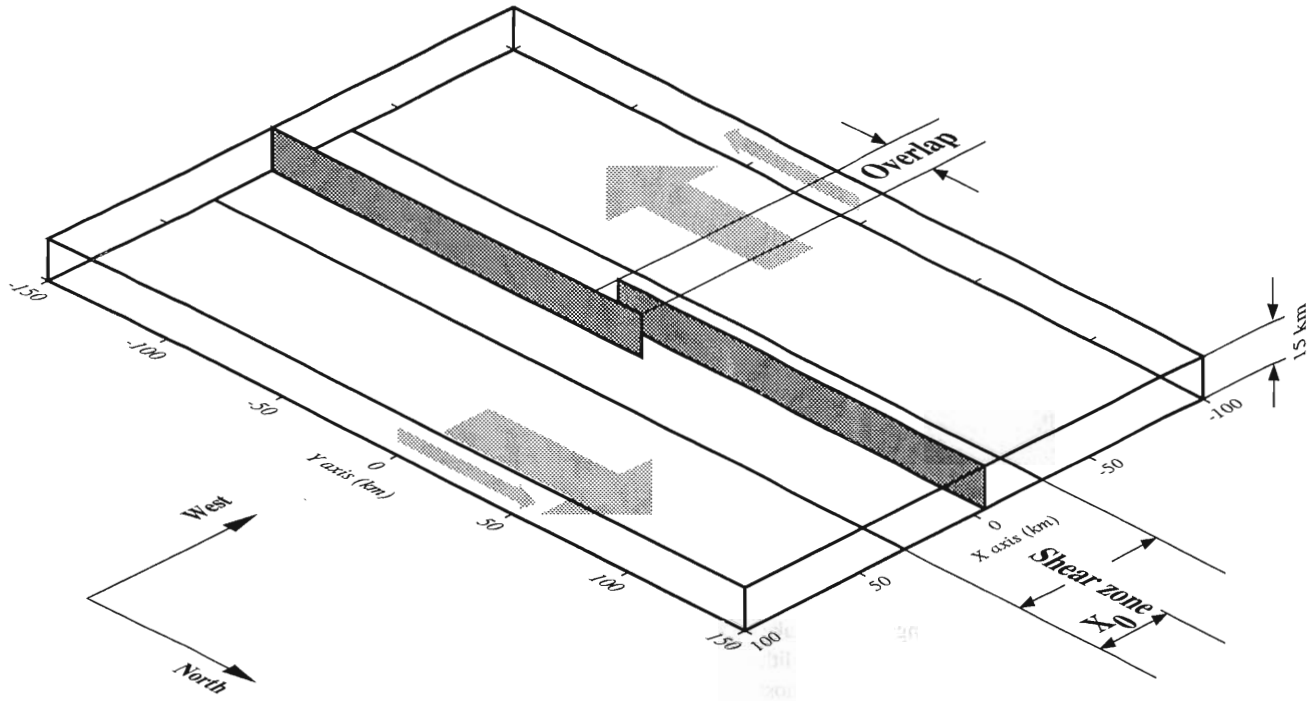

Figure 2. Three-dimensional block diagram showing the geometry of the pull-apart basin model. Shaded surfaces define zones of weakness (faults) having zero shear strength; shaded arrows indicate displacement defined as boundary conditions. The base of the model in the vicinity of the faults (the shear zone) is stress free and thus freely deforming. The width of the shear zone, $2x_0$, and the overlap between faults are varied in the models that follow.

Therefore, we do not attempt to predict absolute uplift, subsidence, or slip along faults but only a relative pattern of deformation.

Since we are dealing with linear analysis, scaling of the input displacement implies the same scaling to the output displacement; therefore, there is no need to use the exact slip that is measured in the field. Also, since displacement (and not stress) boundary conditions are applied, increasing Young's modulus by some factor will not affect the resulting displacement, but will increase the resulting stress by the same factor without changing its pattern.

The Dead Sea Basin, Geological Background

The Dead Sea Basin is located along the Dead Sea Rift, which is a transform boundary separating the African and the Arabian plates (Figure 3). The left lateral motion along the Dead Sea transform probably started at 11 to 15 Ma and shows an offset of 105 km [*Joffe and Garfunkel*, 1987]. About 30 km of this offset occurred in the last 5 m.y., which is also the maximum age of the basin. Since the zone of lithospheric extension in the Dead Sea Basin is quite narrow (about 10 km wide, which is approximately the width of the basin), most of the thermal perturbation due to stretching at the center of the basin is expected to dissipate laterally during the stretching phase [*ten Brink et al.*, 1993]. Therefore, "post-rift" thermal subsidence can be neglected, and the development of the Dead Sea Basin can be studied by mechanical modeling. The relatively simple structure of the Dead Sea Basin together with its large dimensions provides an excellent example for this study.

The structure of the Dead Sea Basin presented here is based mainly on a recent extensive gravity study of the basin [*ten Brink et al.*, 1993]. This recent study indicates that the basin is a full graben 132-km long, 7- to 18-km wide, and 10-km deep, with no boundary faults at its northern and southern ends (Figure 4). The gravity data also indicate that the Moho is not elevated beneath the basin, so that the basin appears to be locally uncompensated. The symmetry of the basin is also supported by seismic reflection data [*ten Brink and Ben-Avraham*, 1989]. The eastern and western flanks of the basin are not elevated above the regional elevation of the transform flanks. Earthquake focal mechanism data are limited but may indicate some overlap between the strike-slip faults bounding the Dead Sea [*van Eck and Hofstetter*, 1989] (Figure 4).

Tectonic Modeling for Deep Pull-Apart Basins

We suggest a mechanism in which the motion of the upper crust is driven from below by the shear motion of the lower crust and the upper mantle. The driving shear at the base of the upper elastic crust is modeled by a displacement that is specified on the bottom of the model. Because we are dealing with deep basins, the assumption is that the primary faults penetrate the entire upper crust (Figure 2).

Shear at the base of the upper crust is represented by a displacement of 2.5 km in the positive y direction (northward) on part of the bottom of the eastern plate ($z = 15$, $x > x_0$) and a negative y displacement (southward) of 2.5 km on part of the bottom of the western plate ($z = 15$, $x < -x_0$), where x_0 represents the half width of the shear zone. The same displacement is applied on the eastern and western walls of the models (Figure 2). Wherever the y displacement is defined, zero displacement in the x and z directions is explicitly defined as well. We do not define the displacement at the base of the

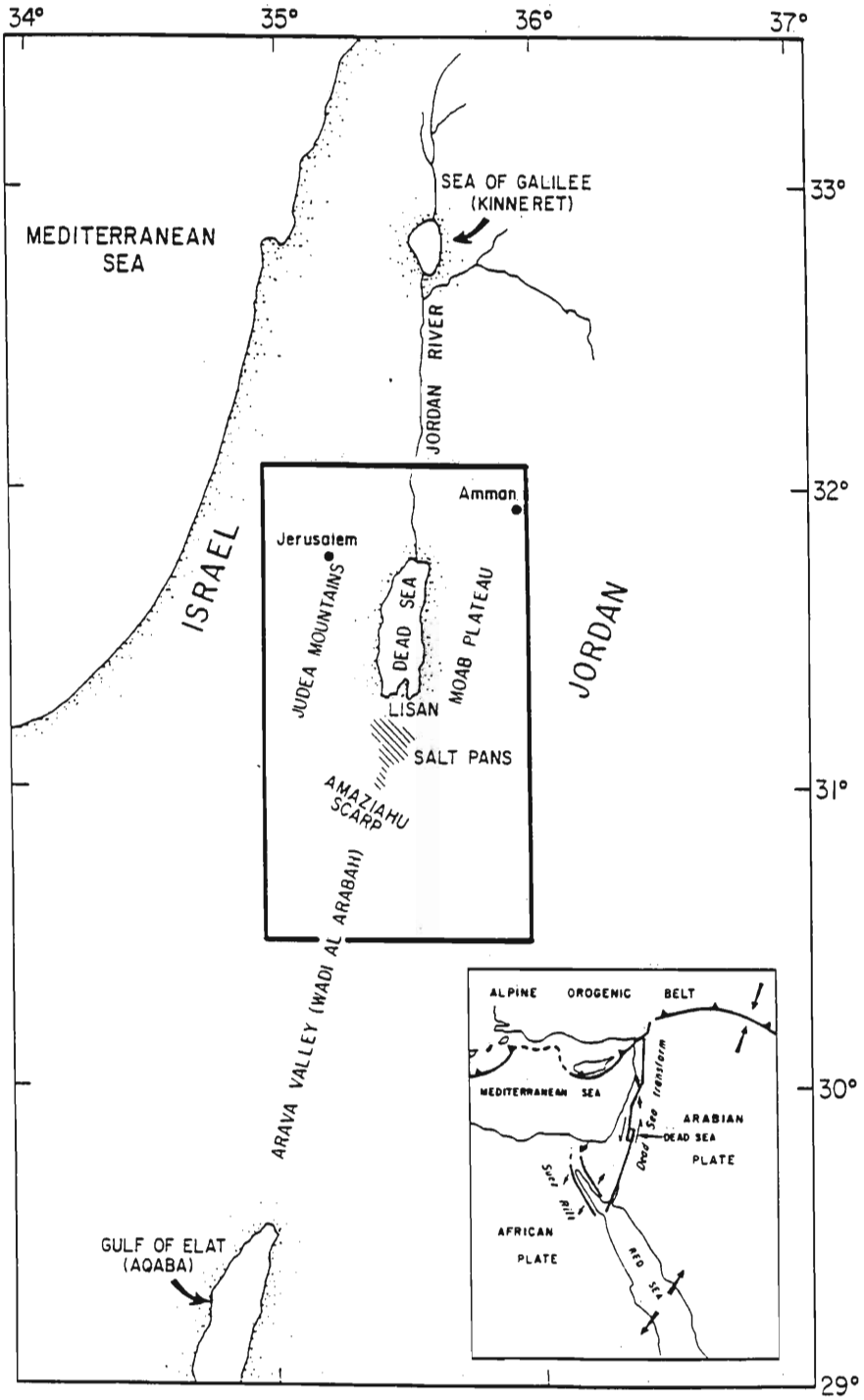

Figure 3. Location map of the Dead Sea Basin. Inset: Configuration of tectonic plates. (From *ten Brink et al.* [1993].)

upper crust in the vicinity of the faults, i.e., at the shear zone ($-x_0 \leq x \leq x_0$, Figure 2).

Based on geological and geophysical observations and physical models, several authors have argued that detachment surfaces underlie some strike-slip faults [e.g., *Terres and Sylvester*, 1981; *Royden*, 1985; *Nicholson et al.*, 1986; *Bird et al.*, 1987; *Hudnut et al.*, 1988; *Namson and Davis*, 1988; *Richard and Krantz*, 1991]. Thus, we assume that the base of the upper crust beneath the pull-apart basin is detached from the lower crust and can adjust itself by moving in all directions including vertically (free surface boundary conditions).

Pull-apart basins are modeled here by two semi-infinite en echelon vertical planes of weakness, representing faults, that penetrate the entire thickness of a 3-D elastic plate (Figure 2). No shear (tangential) stress is allowed to develop on the faults. The width (x), length (y), and depth (z) of the plate are 200, 300, and 15 km, respectively. The faults are oriented in the y direction and are 10 km apart with zero overlap (unless noted

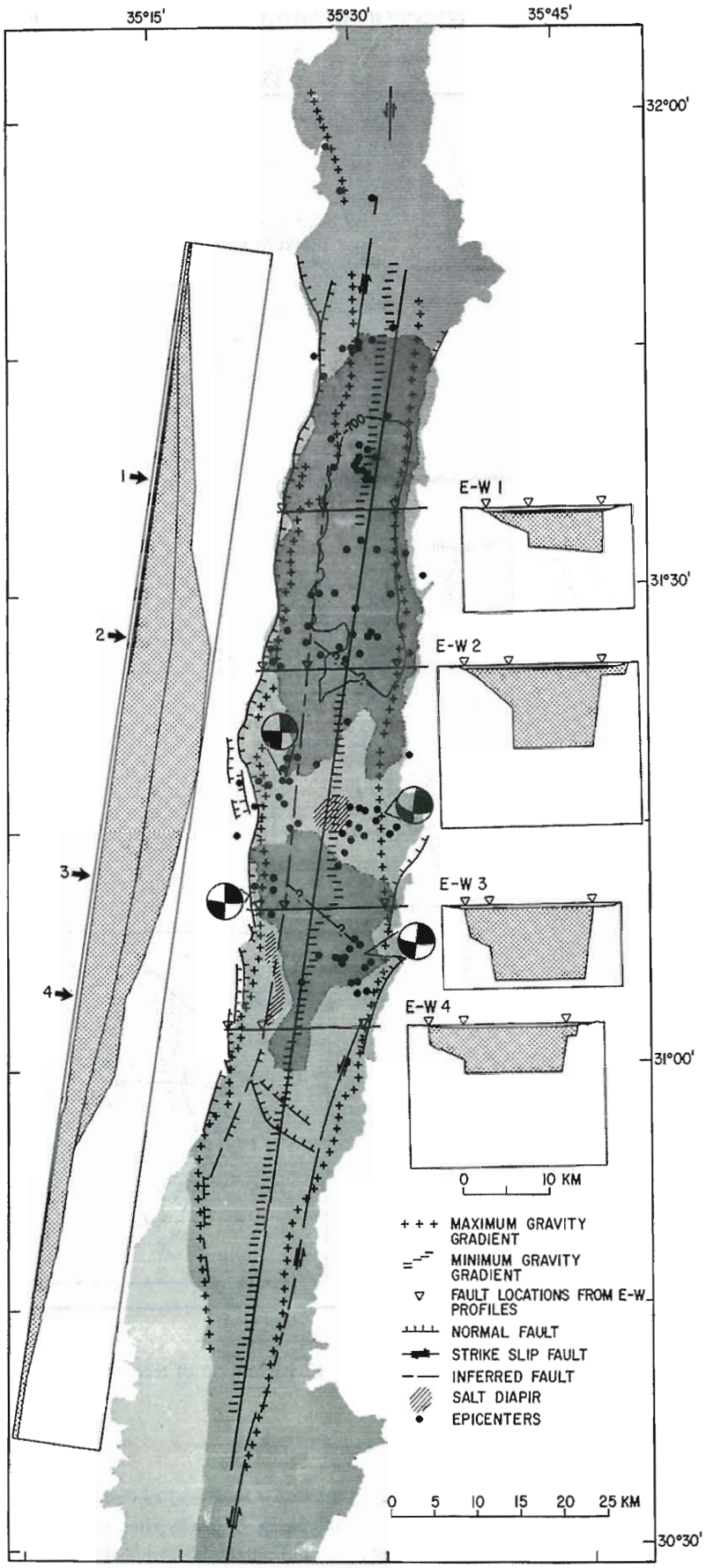

Figure 4. Structural interpretation of the Dead Sea Basin. Solid lines mark locations of profiles. The four east-west profiles are based on 2-D gravity modeling. The along-axis profile is based on 2 1/2-D gravity modeling. Also included are fault plane solutions (balls), epicenter locations (dots), and surface faults. Dark shading marks lake and salt pans (From *ten Brink et al.* [1993].)

otherwise). We chose a fault length of 150 km to minimize the edge effects that might otherwise affect the structure at the center of the model where the pull-apart basin is developed. Each fault is characterized by two sets of elements that separate between two distinct zones. Free surface boundary conditions are defined on the upper surface as well as on the northern and southern walls of the model (the walls were chosen far enough away so that the boundary conditions on them would not affect the deformation pattern close to the basin). The Young's modulus in all models was 75 GPa. In order to conserve volume over the geological timescale that is considered here, a Poisson's ratio of 0.5 was chosen. In appendix B we investigate the effect of Poisson's ratio on the surface deformation.

Because finite displacement boundary conditions (up to several kilometers) are used in a linear elastic rheology, the stresses that occur are many orders of magnitude larger than the stresses that can be supported within the Earth. We are therefore unable to incorporate processes that involve stress-related boundary conditions, such as isostatic response to sediment loading or friction on faults. As to the isostatic effects, *ten Brink et al.* [1993] showed that the Dead Sea Basin is likely to be uncompensated owing to the small width of the basin with respect to the lithospheric elastic thickness; therefore, isostatic response to sediment loading is not an important factor in the Dead Sea Basin development. In cases where the isostatic effect is important, it can be calculated separately and then added to the faulting solution. As for shear stresses on the faults, the assumption of weak faults is supported by low heat flow above major strike-slip faults like the San Andreas [*Lachenbruch and Sass*, 1980] that indicate shear stresses of an order of magnitude smaller than that predicted by application of Byerlee's law [*Molnar*, 1992]. Heat flow data in the Dead Sea, although not as reliable as in the San Andreas, show values that are comparable with average continental values [*Ben-Avraham et al.*, 1978; *Eckstein and Simmons*, 1978] and therefore indicate that there are no high shear stresses on the faults.

In the following, we first examine the deformation of deep pull-apart basins as a function of the width of the shear zone at the bottom of the upper crust and as a function of the overlap between the en echelon faults. Then, we apply these results to the Dead Sea Basin.

Effect of Shear Zone Width on Pull-Apart Basins

We first explore the effect of changing the width of the shear zone ($-x_0 \leq x \leq x_0$) on the deformation of the basin. The model results for shear zones 10, 20, and 40 km wide (Plates 2a-2c) are also compared with a model similar to that of *Rodgers* [1980] where a constant slip is applied directly on the faults (Plate 2d).

In all the models that are driven by basal motion (Plates 2a-2c), the offset across the faults decreases toward the fault tips, so that a natural tapering of the fault slip function is obtained. However, significant differences are observed between the results of various shear zone widths. The basin is smeared (i.e., gets longer and wider) and becomes shallower as the width of the shear zone increases. A close examination of Plates 2a-2c reveals two additional differences close to the fault tips: (1) rotation of the grid (both outside and inside the basin) is smaller when the shear zone at the bottom is wider; and (2) slip on the faults tapers more rapidly toward the tips when the shear zone is narrow, as can be seen from grid offset.

The different basin shapes can be better compared in a cross section in which the maximum subsidence (i.e., vertical displacement at the top of the plate) is normalized to one unit (Figure 5a). As in Plate 2, the basins that develop in response to a wider shear motion at the bottom are spread over a larger area. The results of Figure 5a suggest that if shear in the lower crust occurs over a wider zone, the upper crust will lose its foundation over a larger area, and fault displacement along strike will be less abrupt. It is important to emphasize the different deformation shape of the dislocation model (Plate 2d, Figure 5a) where the high gradients at the center suggest a basin that is extremely deep, is concentrated very close to the fault tips, and has no significant deformation elsewhere.

Although the surface deformation varies significantly with the width of the shear zone, the necking profiles, which represent the sum of the deformation at the top and at the bottom of the plate, are almost identical for different widths of the shear zone (Figure 5b). The true morphology of deep 3-D pull-apart basins is more related to the surface deformation than to the necking profile. In contrast, surface deformation in 2-D models, where displacement is applied only on the sidewalls, is simply half the necking profile and does not depend on the width of the shear zone (Figure 5c).

Effect of Fault Overlap on Pull-Apart Basins

The models that are considered here include two en echelon faults having (1) no overlap between them, (2) overlap that is equal to the fault separation (i.e., 10 km), and (3) overlap that is twice the fault separation (i.e., 20 km). The width of the shear zone at the bottom (Figure 2) for all the models is 40 km. For comparison, we calculated a dislocation model with 20 km of fault overlap as well.

Plates 3a-c show the vertical displacement over the deformed shape of the basin for the three bottom-driven models. The differences between them are (1) the basin is a full graben between the overlapped faults, (2) uplift decreases when overlap increases, and almost no uplift is observed when the overlap is 20 km (Plate 3c), and (3) patterns of rotation are different for different amounts of overlap.

The dislocation model produces different results. The vertical displacement field at the surface for a dislocation model having a 20-km overlap shows two completely separated basins that develop near the fault tips (Plate 3d), in agreement with *Rodgers* [1980]. In addition, significant uplift occurs outside the basin (Plate 3d). These differences are even more prominent in cross sections of the surface vertical displacement (Figure 6). A dislocation model with 20-km overlap produces a half-graben basin between the two faults, in contrast to the full graben that develops for the bottom-driven model with a similar overlap (Figure 6c). For the bottom-driven models, the basin is a full graben over the entire overlap zone (Figures 6b and 6c) and becomes a half graben just outside the overlapping area (Figures 6d and 6e). These observations have direct implications for the structure of the Dead Sea Basin, as we will show in the next section.

In addition to surface deformation, a significant difference in the pattern of rotation around a vertical axis is observed in the vicinity of the basin for the various models. The blocks near the fault tips are subjected to larger rotation when there is less overlap (Plate 4). The largest rotation appears in the basin with zero overlap and has a counterclockwise direction (Plate 4a), as expected from the relative plate motion. As the overlap increases to 10 km, the rotation centers become smaller and more separated (Plate 4b). When the overlap

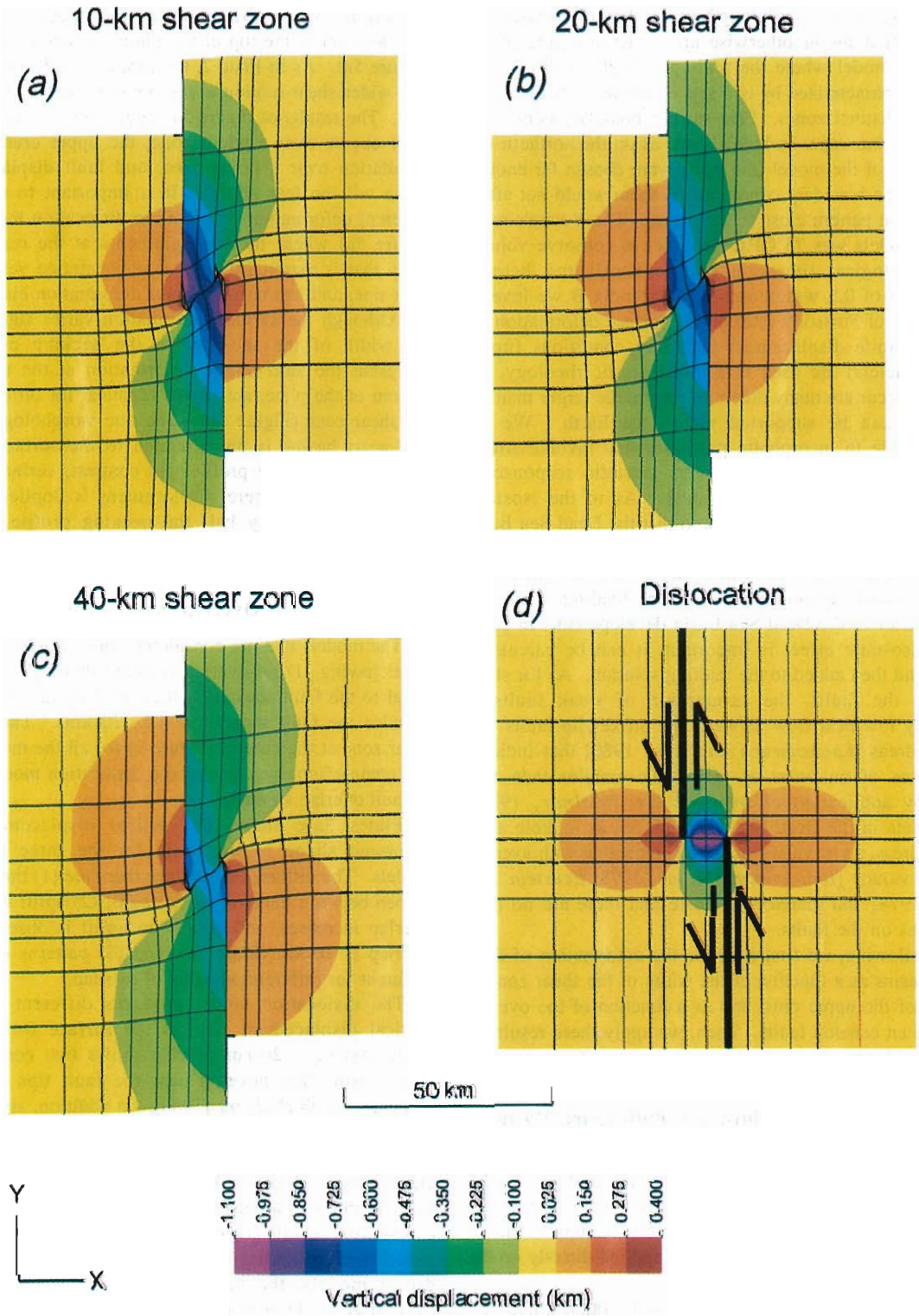

Plate 2. Comparison between 3-D models of pull-apart basin having different shear zone widths and no overlap between the en echelon faults. Vertical displacement (color contours) and horizontal deformation of initially rectangular grid lines in the vicinity of the fault tips are shown for three different widths of shear zone at the bottom: (a) 10 km, (b) 20 km, and (c) 40 km. Left-lateral basal displacement of 5 km (2.5 km on either side) is applied in all of these models (see Figure 2). The horizontal deformation in Plates 2a-2c is multiplied by a factor of 4 to enhance the pattern near the fault tips. (d) Result for a model with the same geometry, in which left-lateral dislocation of 5 km is defined directly on the faults (heavy lines). (The contour plot in Plate 2d is plotted over non deformed elements because the elements near the fault tips are too distorted.)

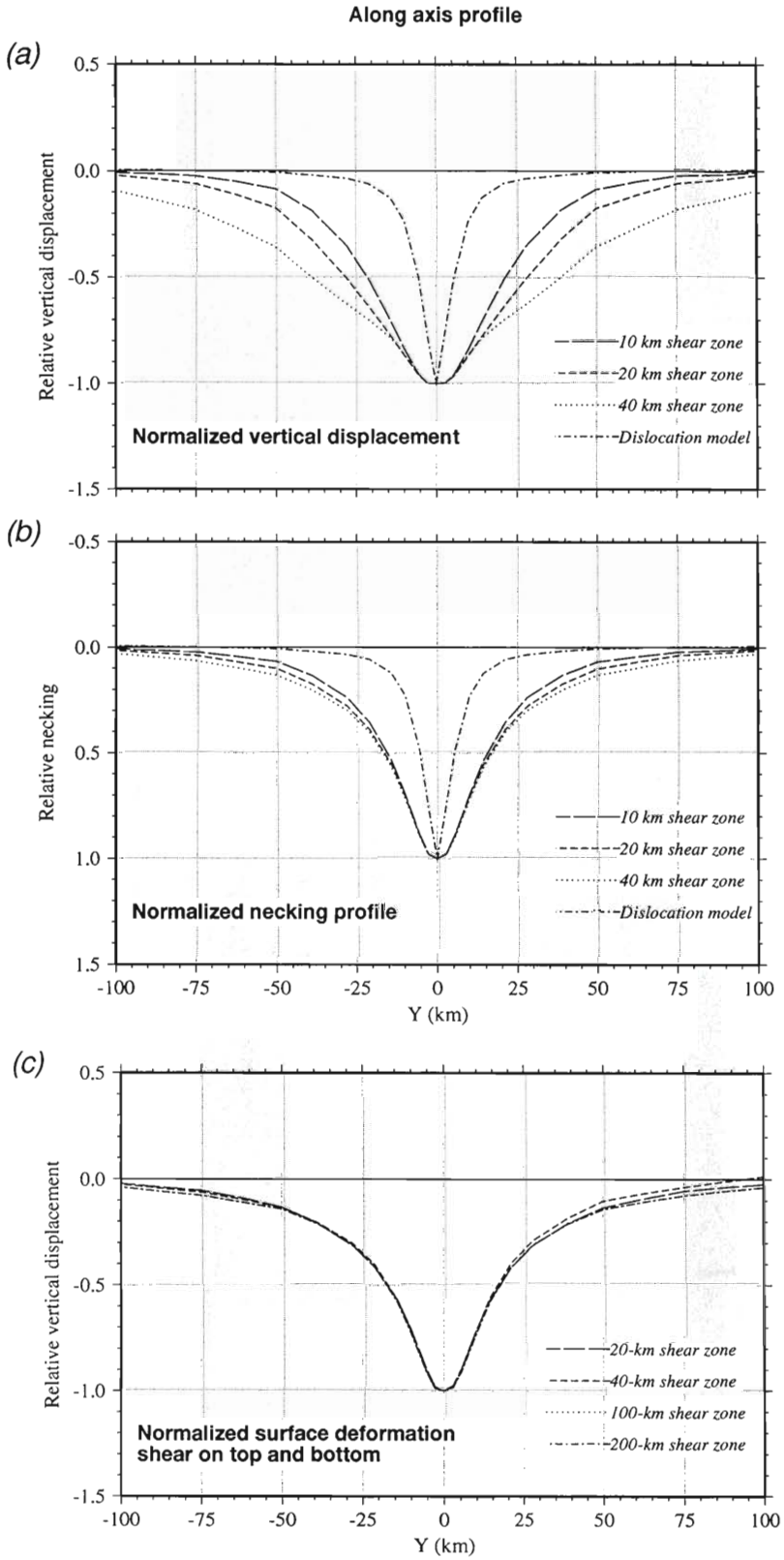

Figure 5. (a) Relative vertical displacement at the surface along axis ($x = 0$) of the models in Plate 2; the maximum subsidence in all models is normalized to one unit. (b) Relative necking profile defined as the absolute sum of the vertical displacement at the top and at the bottom after normalization. Note that all bottom-driven models have a similar necking shape. (c) Relative vertical displacement at the surface for the case in which displacement is applied both on the top and on the bottom surfaces (or on the sidewalls), at different distances from the faults. This model geometry also illustrates a 2-D model with different width of shear zones. Note that the surface vertical displacement here does not depend on the width of the shear zone and represents half of the necking.

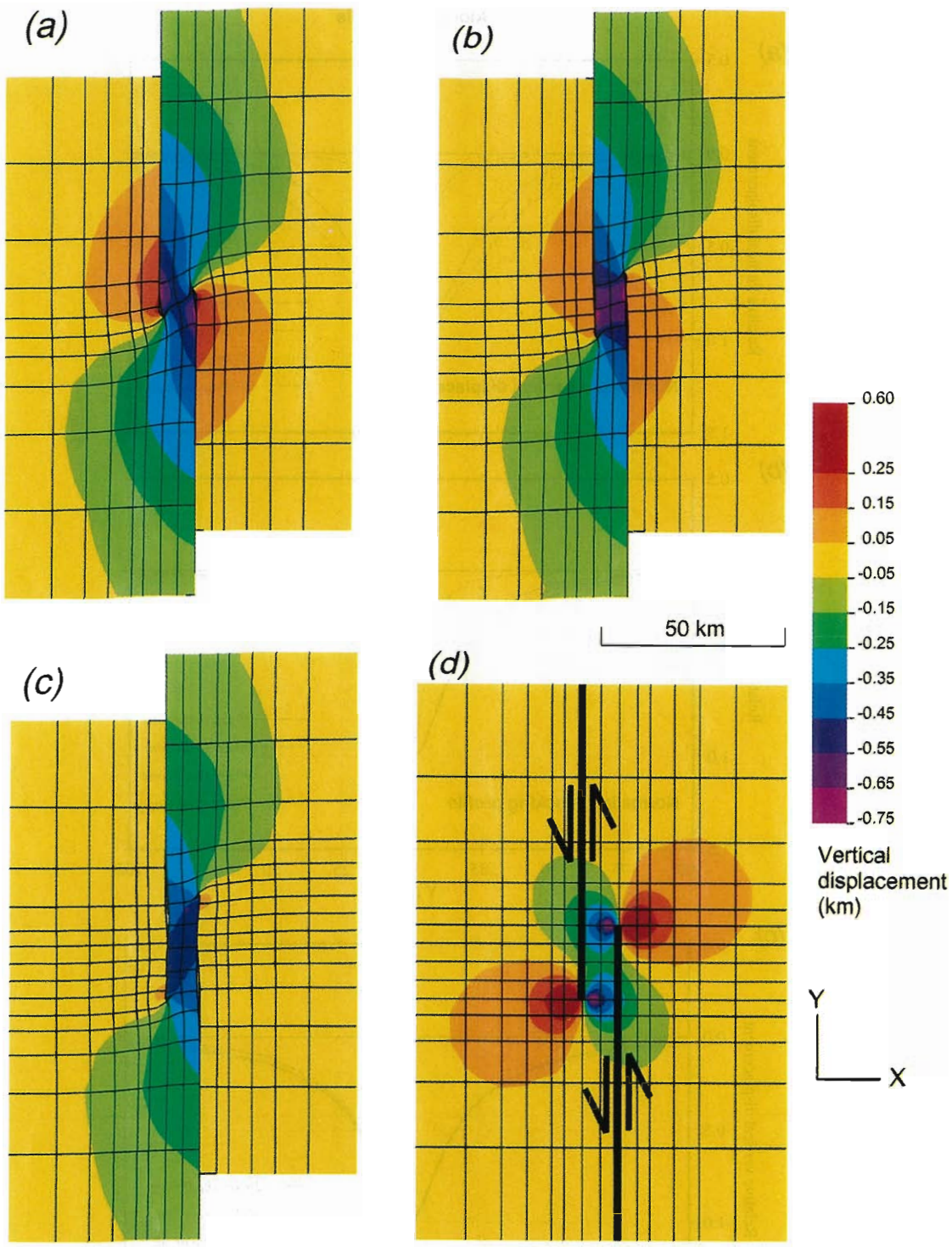

Plate 3. Comparison of 3-D models for a pull-apart basin having different amounts of overlap between the en echelon faults: (a) no overlap, (b) 10-km overlap, which is equal to the separation between the faults, and (c) 20-km overlap. Vertical displacement (color contours) and horizontal deformation of initially rectangular grid lines are due to a left-lateral basal displacement of 5 km (2.5 km on either side). The width of the shear zone at the bottom of the plate is 40 km (see Figure 2). The horizontal deformation in Plates 3a-3c is multiplied by a factor of 4 to enhance the pattern near the fault tips. (d) Result for a model having a 20-km fault overlap in which a left-lateral dislocation of 5 km is defined directly on the faults (heavy lines). (The results in Plate 3d are plotted over nondeformed elements because the elements near the fault tips are too distorted.

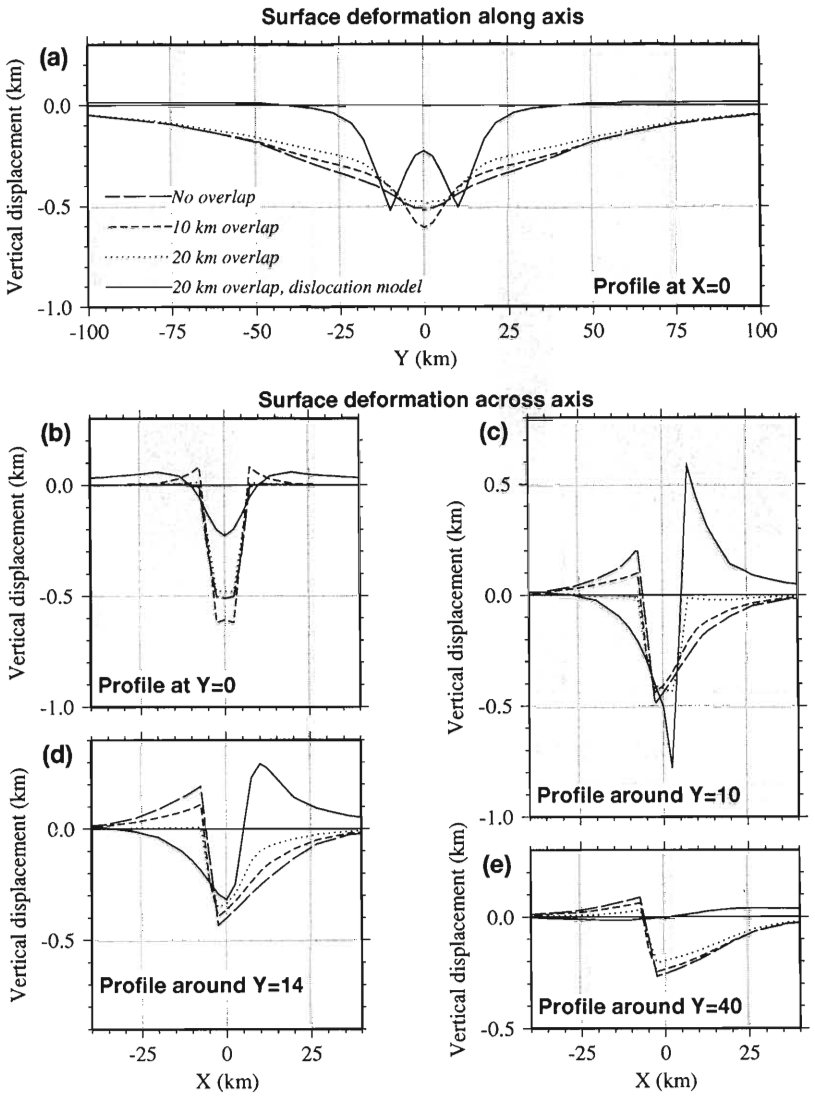

Figure 6. Cross sections of vertical displacement at the surface for the models shown in Plate 3: (a) along the strike of the basin ($x = 0$), and perpendicular to the basin strike at (b) the center of the overlap area ($y = 0$), (c) 10 km from the center, (d) 14 km from the center, and (e) 40 km from the center. Definition of curves for all panels is given in Figure 6a.

reaches 20 km, two completely separated counterclockwise rotation centers develop close to the fault tips, outside the overlap zone, while blocks within the basin are subjected to negligible rotation (Plate 4c). Our interpretation for this phenomenon is as follows. Simple shear and counterclockwise rotation develop near the fault tips in every one of our models (Plates 3a-3c and 4a-4c) because of gradual transition in horizontal displacements from being on a weak fault to a cohesive elastic medium. However, when the overlap increases, the basin is bounded on both sides by planes of weakness that can support no shear. As a result, we obtain partial slip on the faults that bound the basin, whereas the basin itself undergoes no rotation or shear. If this analysis is true, then the lack of rotation and simple shear inside deep pull-apart basins may imply weak basin boundary faults with significant overlap and a decoupled weak substratum. In this case, the blocks that constitute the basin will be subjected to pure extension along the orientation of the faults. In contrast, if uniform rotation occurs between the overlapping faults, then the faults must be able to sustain significant friction stresses, or else shear must develop at the bottom [cf. *Jackson and Molnar*, 1990].

Implications for the Tectonics of the Dead Sea Basin

The morphology of the Dead Sea Basin does not support the simple dislocation model (e.g., *Rodgers* [1980], and Plates 2d and 3d) where a constant slip is defined on the faults. This dislocation model produces a very localized basin (Plate 2d), whereas the Dead Sea Basin stretches over more than 100 km along its strike (Figure 4). Furthermore, the dislocation model predicts extensive subsidence only in an area of about 10 km from the center (Plate 2d, and Figure 5a). In contrast, 50 km from the center of the Dead Sea Basin along strike, the amplitude of subsidence is still 20% of that in the center of the basin (Figure 4). The observations are more consistent with the bottom-driven models having 20- and 40-km-wide shear

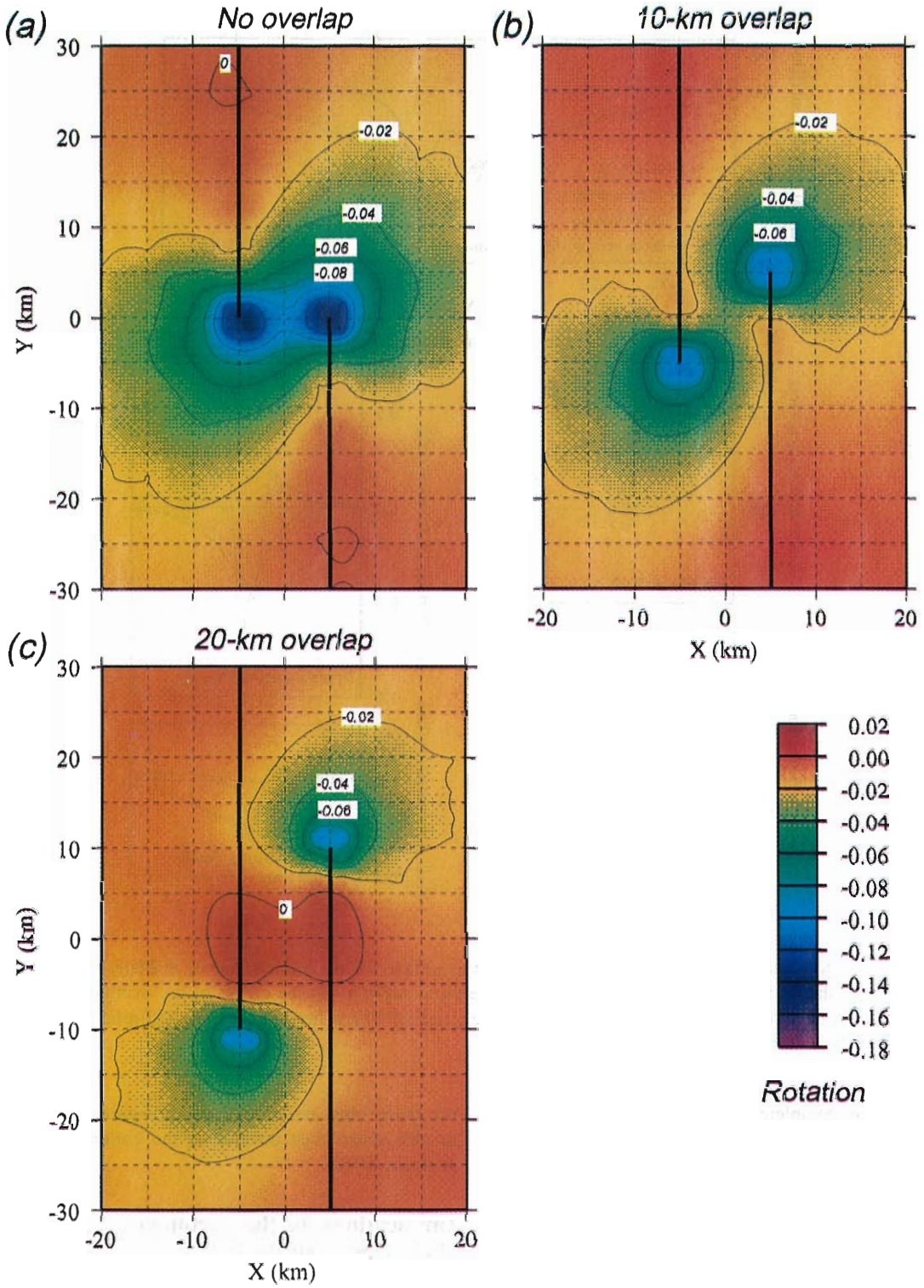

Plate 4. Contour map of the rotation field around a vertical axis as a function of the fault overlap for the models shown in Plates 3a-3c: (a) no overlap, (b) 10-km overlap, and (c) 20-km overlap. Rotation scale is in radians (negative values represent counterclockwise rotation); contour interval is 0.02 rad.

zones (Plates 2b and 2c and Figure 5a), which show that at a distance of 50 km from the center, the subsidence is 17% and 35% of the maximum subsidence respectively. However, these models predict an asymmetric structure (half graben) over the entire length of the basin except at the center (Plates 2b and 2c), in sharp contrast to the full-graben structure of the Dead Sea Basin (Figure 4). In addition, all of the models produce significant uplift at the flanks of the basin near the fault tips, whereas there is no evidence for any localized uplift on the shoulders of the Dead Sea Basin.

When overlap between the faults is considered, a full graben is obtained between the two faults along the entire

overlap (Plates 3a-3c and Figures 6b and 6c). The uplifts on the flanks near the fault tips decrease and completely disappear when the overlap exceeds 20 km (Plates 3a-3c and Figure 6). These features are in agreement with the Dead Sea Basin structure. A dislocation model (constant slip on faults) with overlap is not a good solution because it predicts two separate centers of subsidence near the fault tips and a highly asymmetrical structure with significant uplift at the flanks (Plate 3d).

The four east-west profiles in Figure 4 indicate that the Dead Sea Basin is a full graben over a distance of 50 km from north to south. It is unlikely that the Dead Sea Basin was bounded by two faults with an overlap of 50 km during its initial stage of formation. Results obtained by using a model with 50 km overlap and a 40-km-wide shear zone at the bottom show a full-graben basin along the entire length of the overlap (Plate 5; dashed line in Figure 7) and no significant uplift at the flanks, in agreement with the Dead Sea Basin morphology. Yet the subsidence profile along the axis (dashed line, Figure 7a) is distributed quite differently from the subsidence in the Dead Sea Basin (Figure 4). A better agreement with the Dead Sea Basin morphology is obtained by superposition of the deformation profiles of models with an increasing amount of overlap (solid line, Figure 7). The basin, in this case, appears as a full graben over more than 40 km (from $y = 20$ to $y = -20$); the relative subsidence distribution along the axis is quite similar to the Dead Sea Basin (Figure 4); and no significant uplift is developed on the shoulders of the basin (Figures 7a-7d).

In summary, we suggest that a plausible explanation of the Dead Sea Basin characteristics is that the basin growth is driven by shear that is distributed horizontally over 20 to 40 km at a depth of about 15 km and that the overlap between the en echelon weak faults in the upper crust increases to over 30 km as the basin grows.

Summary

Many geophysical and geological observations support the idea that the lower crust and the upper mantle cannot be decoupled from deformation processes that occur in the upper crust [*Molnar*, 1992]. In this paper we have considered a model in which the upper crust is driven from below by the regional lithospheric plate motion. We have tried to relate the morphology of deep pull-apart basins (in strike-slip settings) to the regional shear at the base of the upper crust and to the geometry of the primary faults that bound the basin. The boundary element method was used to calculate the displacement field in a three-dimensional elastic plate. The faults that bound the basin were defined by two vertical en echelon planes of weakness that penetrated the entire plate. The regional lithospheric plate motion was represented by displacement boundary conditions on the bottom of the elastic plate.

Probably the main reason that no extensive work has been done to simulate numerically the deformation in strike-slip settings that are driven from below by shear motion is the highly three-dimensional nature of the problem. Two-dimensional plane stress modeling produces unrealistic subsidence and uplift close to the fault tips because plane stress approximation assumes no vertical stresses. In contrast, in the 3-D solution significant vertical stresses are developed within the plate near the fault tips, preventing the large deformation there.

When displacement is applied on the bottom of a broken elastic plate, a natural tapering in the fault slip toward the tips is always obtained. The deformation pattern is dependent on the width of the shear zone. When the width of the shear zone increases, the surface deformation gets wider and longer but also shallower, and block rotation both outside and inside the basin decreases.

The amount of overlap between the two primary faults is a significant factor in controlling the morphology of pull-apart basins. When shear is applied from the bottom, a full graben is developed in the overlap zone between the two faults. The uplift just outside the basin near the tip of the faults decreases as the overlap increases. For a model in which the overlap is twice the separation, almost no uplift is developed. These

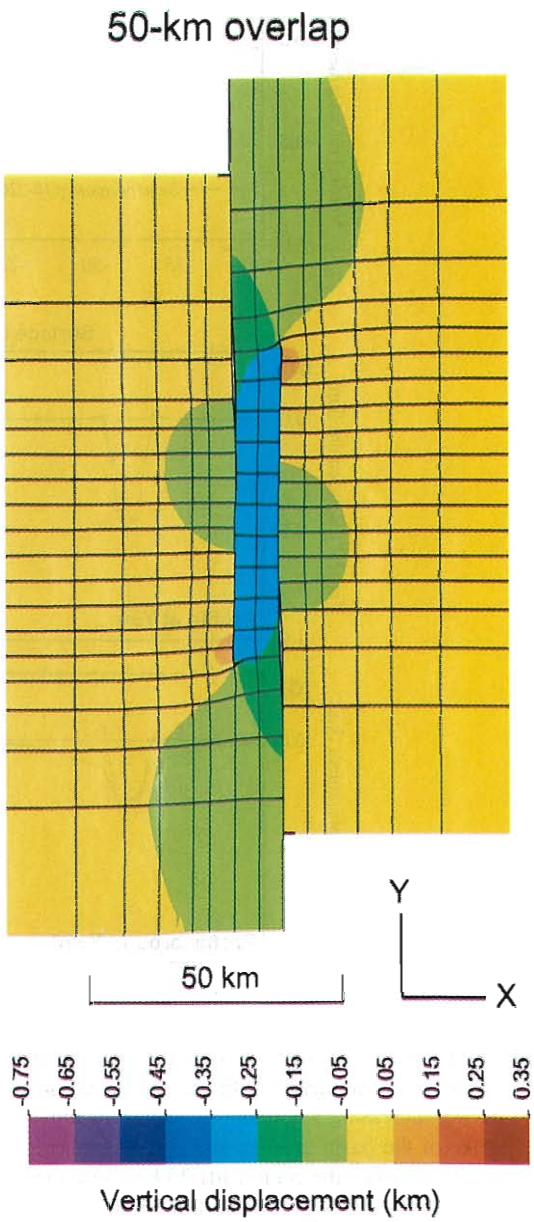

Plate 5. Vertical displacement (color contours) and horizontal deformation of initially rectangular grid for a 3-D pull-apart basin model having an overlap of 50 km (5 times the separation). Left-lateral basal displacement of 5 km (2.5 km on either side) with shear zone of 40 km is applied (see Figure 2). The horizontal deformation is multiplied by a factor of 4 as in Plates 2 and 3.

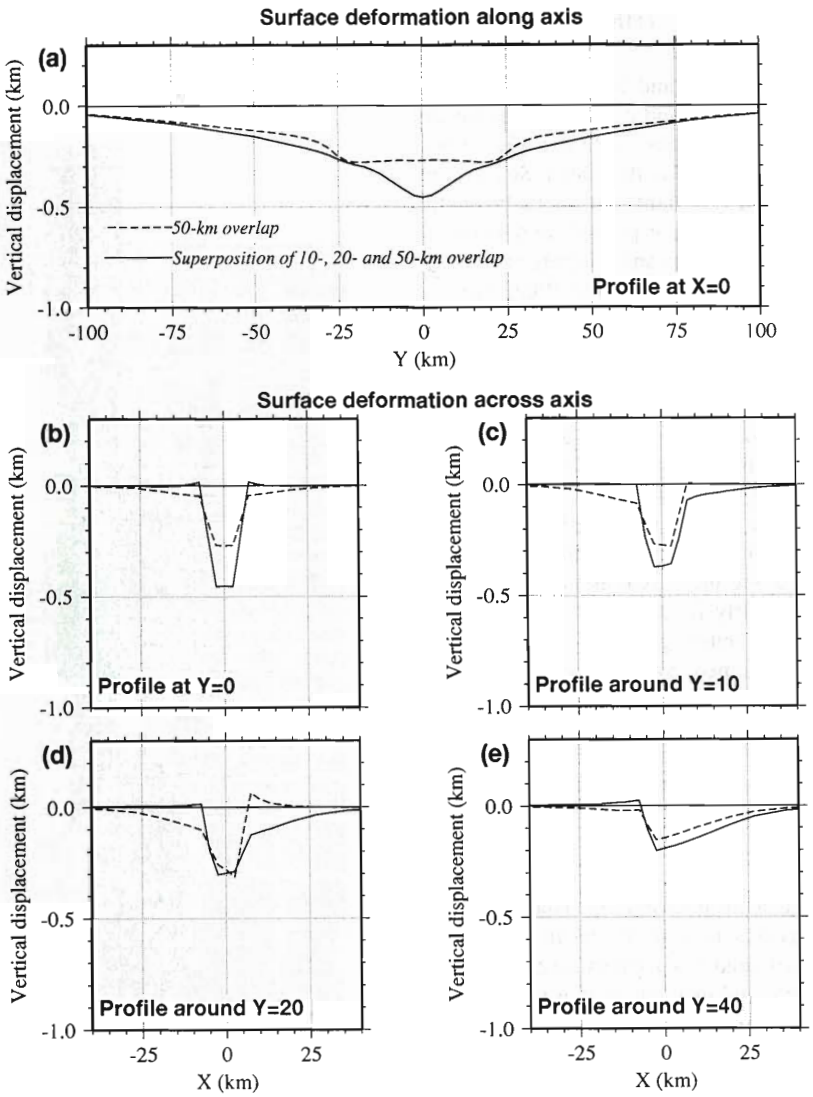

Figure 7. Cross sections of the surface vertical displacement for a model having a 50-km fault overlap (dashed line) compared with the surface vertical displacement that results from superposition of three models having increasing amounts of overlap: 10 km, 20 km and 50 km (solid line). Results are shown (a) along the strike of the basin ($x = 0$), and perpendicular to the basin strike at (b) the center of the overlap area ($x = 0$), (c) 10 km from the center, (d) 20 km from the center, and (e) 40 km from the center. Note that the basin in both cases is a full graben up to 20 km on either side of the center.

results are consistent with the observed pattern of deformation in the Dead Sea Basin. The pattern of rotation and shear is also highly dependent on the amount of overlap. For larger overlap, slip along the faults that bound the basin releases the rotation and the associated simple shear within the basin. These results are in contrast to conventional kinematic models that predict severe rotation between offset crustal blocks by assuming friction on the bounding faults or on the bottom of the blocks. The implication is that the amount of rotation within deep pull-apart basins may indicate the strength of strike-slip faults at the boundary of the basin and the coupling of crustal blocks to the substratum.

The full-graben shape of the Dead Sea Basin, the lack of local uplift above the regional transform shoulders, the length of the basin, and the distribution of subsidence along its axis can all be characterized by a 3-D model having more than 30 km of overlap. In contrast, these Dead Sea Basin features are inconsistent with dislocation models [e.g., *Rodgers*, 1980]. The large overlap was probably developed as the basin evolved. The model further suggests a stable shear motion that is distributed laterally over 20 to 40 km at a depth of about 15 km . This is quite a narrow shear zone, which may indicate a rather strong, cool lower crust and upper mantle beneath the Dead Sea Rift. It would be interesting to compare the Dead Sea Basin with some of the large pull-apart basins adjacent to the San Andreas fault and to verify if the morphology of these basins is consistent with the wider shear zone that should be associated with hotter and weaker lower lithosphere in southern California.

Appendix A: Comparison of Analytical and Numerical Results for a Rectangular Dislocation Surface

In order to evaluate the quality of the boundary element algorithm used for this work, we ran a series of models for which the analytical solution is known and compared the numerical and analytical results. We used the analytical solutions that were obtained by *Chinnery* [1961, 1963] for a rectangular vertical surface across which a displacement

discontinuity is defined (Figure 8a). The rectangular dislocation fault is embedded in a semi-infinite isotropic elastic medium. This model was chosen because it emphasize the need for a 3-D analysis.

The analytical results for the model in Figure 8a were calculated at the surface for a Poisson solid ($\lambda = \mu$) and a fault that intersects the surface ($d = 0$). The solution, in this case, is simplified to a nondimensional form (equation 8 of *Chinnery* [1961]), which can be easily programmed. The numerical results, on the other hand, are not as easy to obtain. The geometry of the problem causes severe discontinuities of the displacement and stress fields near the tips of the dislocation surface. The fact that the two tips of the fault are close to each other (relative to the depth of the fault) makes it even harder to

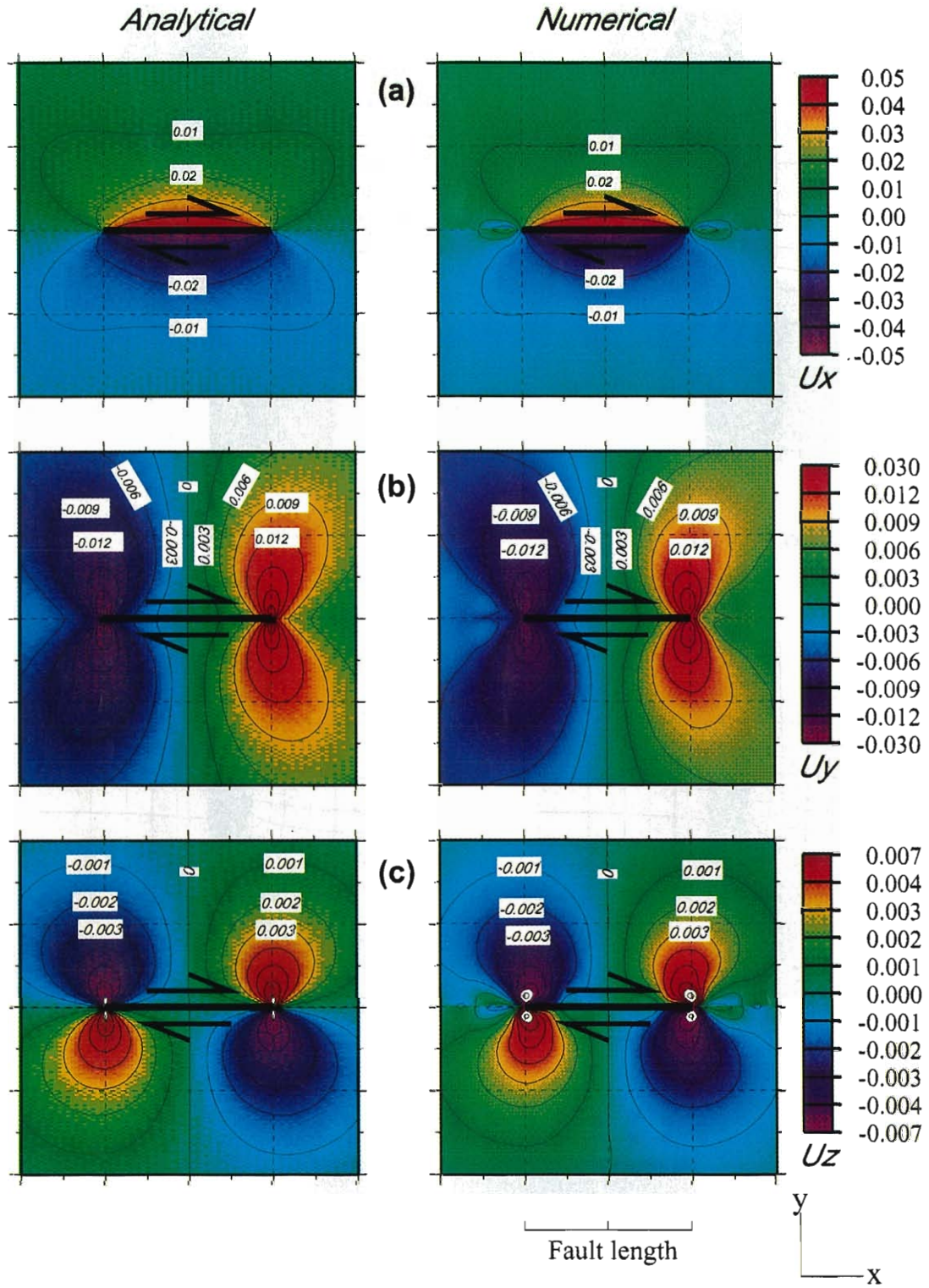

Plate 6. Results for the dislocation model shown in Figure 8. Analytical (left) and numerical (right) displacement in the (a) x direction U_X, (b) y direction U_Y, and (c) z direction U_Z, at the surface ($z = 0$). Heavy line denotes trace of fault.

obtain a numerical solution that will behave similarly to the analytical solution near the fault tips. In Figure 8b we show the distribution of elements that was used to calculate this problem. The elements near the fault tips are small compared with the rest of the elements and are also quadratic; i.e., a three-dimensional quadratic surface can be defined on each one of the elements near the fault tips. The faults themselves are defined by two sets of elements so that one set of elements can be shifted by a finite displacement with respect to the other.

The analytical and numerical results for the displacement field in the x, y, and z directions are similar (Plate 6). The magnitude of the field is the same, and the numerical artifacts

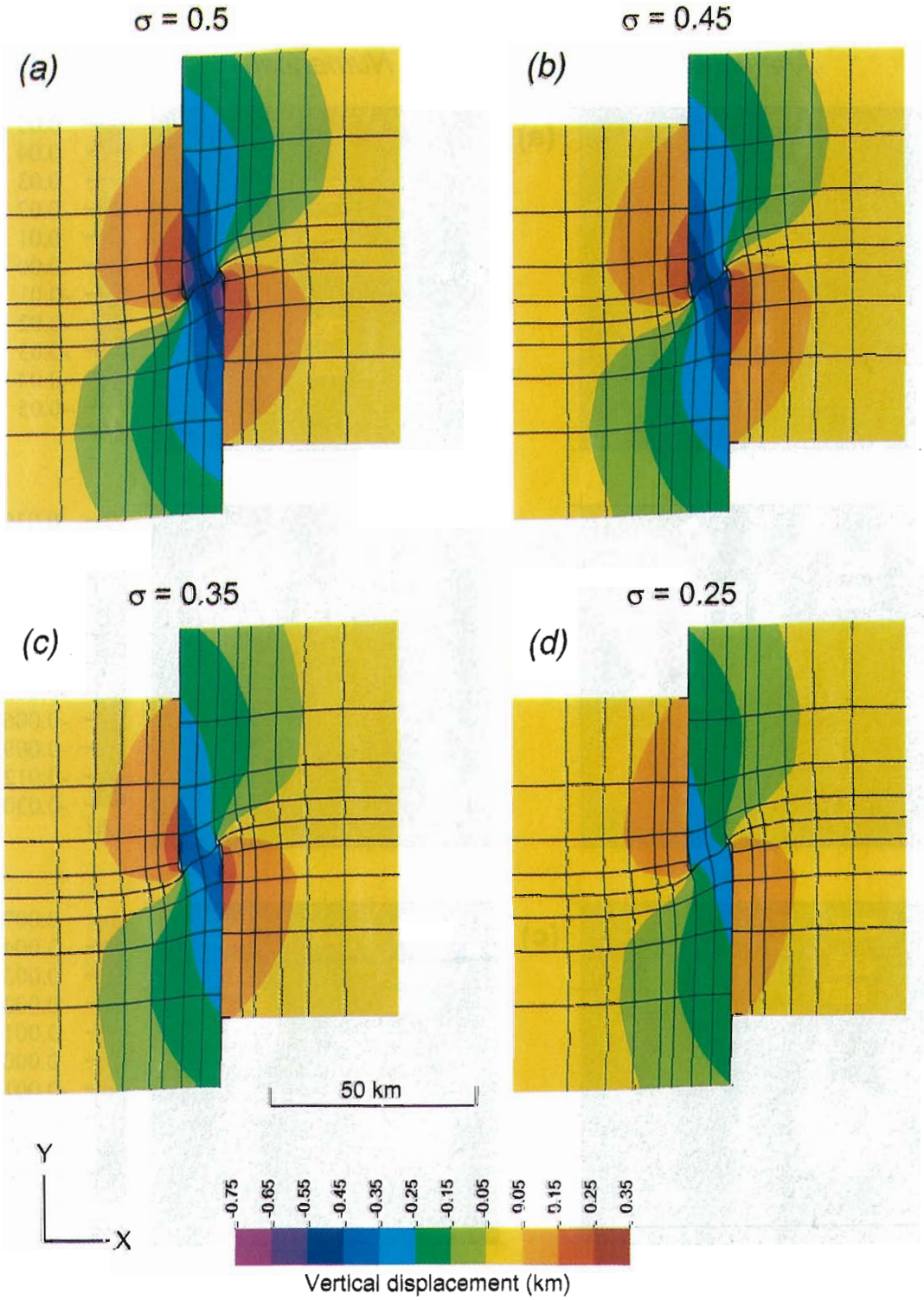

Plate 7. Comparison between 3-D models of pull-apart basin with different Poisson's ratio of (a) 0.5, (b) 0.45, (c) 0.35, and (d) 0.25. Vertical displacement (color contours) and horizontal deformation of initially rectangular grid lines are caused by a left lateral basal displacement of 5 km (2.5 km on either side). The width of the shear zone at the bottom of the plate is 40 km (see Figure 2). The horizontal deformation is multiplied by a factor of 4 to enhance its pattern.

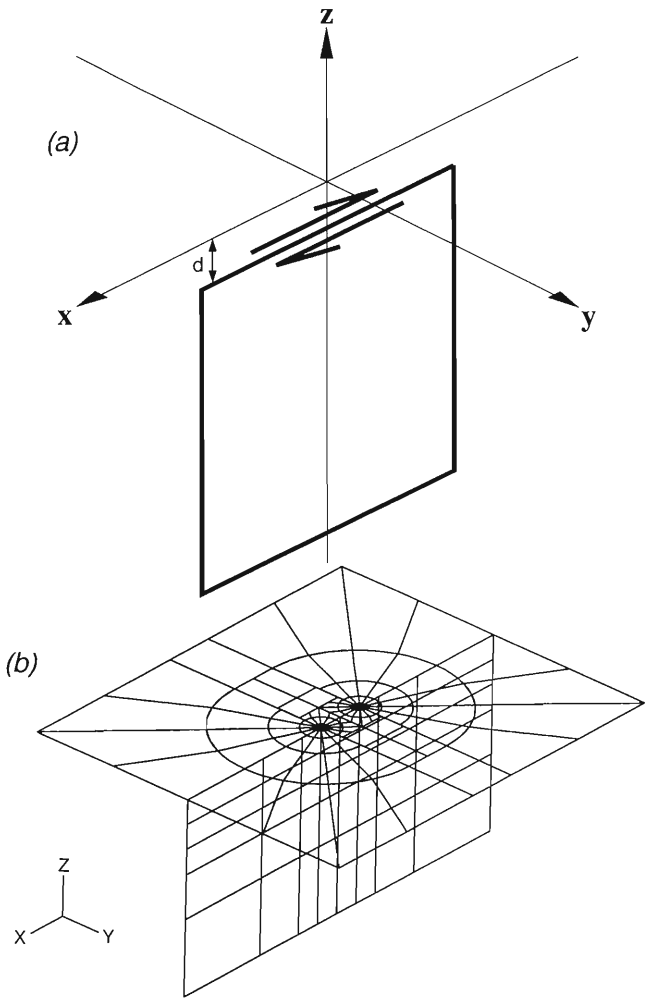

Figure 8. (a) Dislocation of a vertical fault plane of finite depth embedded in an elastic half-space at depth d. This geometry was used to compare the analytical and numerical solutions. (b) Distribution of elements for the rectangle dislocation model shown in Figure 8a.

near the fault tips are small. The same comparison was done for the stress field shown by *Chinnery* [1963], and the results both on the surface and on a plane bisecting the fault were satisfactory.

Appendix B: The Effect of Poisson's Ratio on Surface Deformation

Although solids usually have a Poisson's ratio of 0.25 to 0.3, our models use a Poisson's ratio of 0.5. A Poisson's ratio of 0.5 implies conservation of volume, which is a good assumption for the finite-displacement processes that we attempt to model here. Infinitesimally small displacements are partially accommodated by dilatation or compression, but the finite displacement processes that occur in the upper crust are accommodated by brittle or plastic failure and not by volumetric change.

The infinite incompressibility, which is implied by a Poisson's ratio of 0.5, may potentially cause numerical instabilities. We explore the effect of Poisson's ratio on the surface deformation by running a series of models with the same properties (40-km shear zone, no overlap between the faults) and different values of Poisson's ratio of 0.5, 0.45, 0.35, and 0.25 (Plates 7a-7d).

The results in Plate 7 indicate that the deformation pattern for all the models is the same and does not depend on specific choice of a Poisson's ratio. Also, there is no indication of any special singularities in the results that may be associated with the infinite incompressibility of the model with a Poisson's ratio of 0.5, indicating BEASY can handle this special case well. However, the absolute values of the subsidence and uplift do decrease gradually when Poisson's ratio decreases. Such dependence on Poisson's ratio is expected: for a Poisson's ratio of 0.5, the model response to the basal shear is characterized entirely by surface deformation. As Poisson's ratio decreases, part of the model response would be represented by a volume change and therefore the surface deformation will decrease as shown in Plate 7.

Acknowledgments. Part of this research was done when one of the authors (RK) was a summer intern at ARCO Exploration and Production Technology. We are grateful to C. Ruppel for fruitful discussions and constructive suggestions. R. Stein provided significant, valuable comments on an earlier draft of the manuscript. K. Meisling and R. Krantz kindly provided an unpublished internal report on strike-slip systems. We thank J. Trevelyan from Computational Mechanics for answering numerous questions regarding the BEASY boundary element code, and M. Bott, P. Morgan, R. Bilham, K. Klitgord, and D. Hutchinson for their reviews. This work was supported by the U.S. Geological Survey marine program, NSF grant OCE-9300708, and ONR grant N00014-91-J1433.

References

Ben-Avraham, Z., R. Hanel, and H. Villinger, Heat flow through the Dead Sea rift, *Mar. Geol., 28,* 253-269, 1978.

Bilham, R., and G. King, The morphology of strike-slip faults: Examples from the San Andreas fault, California, *J. Geophys. Res., 94,* 10204-10216, 1989.

Bird, T.J., A. Bell, A.D. Gibbs, and J. Nicholson, Aspects of strike-slip tectonics in the Inner Moray Firth Basin, offshore Scotland, *Nor. Geol. Tids., 67,* 353-369, 1987.

Brace, W.F., and D.L. Kohlstedt, Limits on lithospheric stress imposed by laboratory experiments, *J. Geophys. Res., 85,* 6248-6252, 1980.

Braun, J., Three-dimensional numerical simulations of crustal-scale wrenching using a non-linear failure criterion, *J. Struct. Geol., 16,* 1173–1186, 1994.

Byerlee, J.D., Friction of rocks, *Pure Appl. Geophys., 73,* 615-626, 1978.

Chinnery, M.A., The deformation of the ground around surface faults, *Bull. Seismol. Soc. Am., 51,* 355-372, 1961.

Chinnery, M.A., The stress changes that accompany strike-slip faulting, transform, *Bull. Seismol. Soc. Am., 53,* 921-932, 1963.

Crouch, S. L., and A. M. Starfield, *Boundary Element Methods in Solid Mechanics*, 332 pp., Allen and Unwin, Winchester, Mass., 1983.

Eckstein, Y. and G. Simmons, Measurements and interpretation of terrestrial heat flow in Israel, *Geothermics, 6,* 117-142, 1978.

Gomberg, J., Tectonic deformation in the New Madrid seismic zone: Interface from map view and cross-sectional boundary element models, *J. Geophys. Res., 98,* 6639-6664, 1993.

Gomberg, J., and M. Ellis, Topography and tectonics of the central New Madrid seismic zone: Results of numerical experiments using a three-dimensional boundary element program, *J. Geophys. Res., 99,* 20,299–20,310, 1994.

Hudnut, K., L. Seeber, J. Pachelo, J. Armbruster, L. Sykes, G. Bond and M. Kominz, Cross faults and block rotation in southern California: Earthquake triggering and strain distribution, *Lamont Res. Annu.*, 44-49, 1988.

Jackson, J., and P. Molnar, Active faulting and block rotation in the Western Transverse Ranges, California, *J. Geophys. Res., 95,* 22073-22087, 1990.

Joffe, S., and Z. Garfunkel, Plate kinematics of the circum Red Sea — A re-evaluation, *Tectonophysics, 141,* 5-22, 1987.

Lachenbruch, A.H., and J.H. Sass, Heat flow and energetics of the San Andreas fault zone, *J. Geophys. Res., 85,* 6185-6222, 1980.

Molnar, P., Brace-Goetze Strength profiles, the partitioning of strike-slip and thrust faulting at zones of oblique convergence, and the stress-heat flow paradox of the San Andreas fault, in *Fault Mechanics and Transport Properties of Rocks*, edited by T. F. Wong and B. Evans, pp. 435–459, Academic, San Diego, Calif., 1992.

Namson, J.S., and T.L. Davis, Seismically active fold and trust belt in the San Joaquin Valley, Central California, *Geol. Soc. Am. Bull., 100,* 257-273, 1988.

Nicholson, C., L. Seeber, P. Williams, and L.R. Sykes, Seismic evidence for conjugate slip and block rotation within the San Andreas fault system, southern California, *Tectonics, 5,* 629-648, 1986.

Richard, P., and R.W. Krantz, Experiments on fault reactivation in strike-slip mode, *Tectonophysics, 188,* 117-132, 1991.

Rodgers, D.A., Analysis of pull-apart basin development produced by en echelon strike-slip faults, *Spec. Publ. Int. Assoc. Sedimentol., 4,* 27–41, 1980.

Royden, L. H., The Vienna basin: A thin-skinned pull-apart basin, in Deformation and Basin Formation Along Strike-Slip Faults, edited by K. T. Biddle and N. Christie-Blick, *Spec. Publ. Soc. Econ. Paleontol. Mineral.*, 37, 319-338, 1985.

Segall, P., and D.D. Pollard, Mechanics of discontinuous faults, *J. Geophys. Res., 85,* 4337–4350, 1980.

ten Brink, U.S., and Z. Ben-Avraham, The anatomy of a pull-apart basin: Seismic reflection observations of the Dead Sea basin, *Tectonics, 8,* 333-350, 1989.

ten Brink, U.S., Z. Ben-Avraham, R.E. Bell, M. Hassouneh, D.F. Coleman, G. Andeasen, G. Tibor, and B. Coakley, Structure of the Dead Sea pull-apart basin from gravity analysis, *J. Geophys. Res., 98,* 21887-21894, 1993.

Terres, R.R., and A.G. Sylvester, Kinematic analysis of rotated fractures and blocks in simple shear, *Bull. Seismol. Soc. Am., 71,* 1593-1605, 1981.

van Eck, T., and A. Hofstetter, Microearthquake activity in the Dead Sea region, *Geophys. J. Int., 99,* 605-620, 1989.

R. Katzman, Department of Earth, Atmospheric and Planetary Sciences, Rm. 54-522, Massachusetts Institute of Technology, Cambridge, MA 02139. (e-mail: rafi@quake.mit.edu)

J. Lin, Department of Geology and Geophysics, Woods Hole Oceanographic Institution, Woods Hole, MA 02543. (e-mail: jian@galileo.whoi.edu)

U.S. ten Brink, U.S. Geological Survey, Quinsett Campus, Woods Hole, MA 02543. (e-mail: tenbrink@nobska.er.usgs.gov)

(Received April 8, 1994; revised October 6, 1994; accepted November 29, 1994.)